7th ECCOMAS Thematic Conference on the Mechanical Response of Composites
COMPOSITES 2019
A. Turon, P. Maimí & M. Fagerström (Editors)

ESTIMATING THE AVERAGE SIZE OF FIBER/MATRIX INTERFACE CRACKS IN UD AND CROSS-PLY LAMINATES

Luca Di Stasio[1,2,*], **Janis Varna**[1], **Zoubir Ayadi**[2]

[1] Luleå University of Technology, University Campus, SE-97187 Luleå, Sweden
[2] Université de Lorraine, EEIGM, IJL, 6 Rue Bastien Lepage, F-54010 Nancy, France
[*] luca.di.stasio@ltu.se

Keywords: Fiber Reinforced Polymer (FRP), Debonding, Linear Elastic Fracture Mechanics (LEFM).

Summary: *This document provides information and instructions for preparing the (optional) full-length paper for the COMPOSITES 2019 Conference (September 18-20, 2019 in Girona, Spain).*

1. INTRODUCTION

The Conference publication will consist of a pen drive containing papers of the contributions received and a printed Book of Abstracts containing a one page version of the accepted abstracts. The authors must submit a full-length paper (max. 12 pages) using the same format of this template. Submission of a full-length paper is not mandatory but authors are strongly encouraged to send it before June 27, 2019.

The deadline date for early registration date is April 30, 2019. Presenting authors must register by June 13, 2019. Papers with authors not registered by this date will be removed from the final program. Registration closes on September 5, 2019. Further information can be found at the conference website: www.composites2019.udg.edu

2. RVE MODELS AND FE DISCRETIZATION

In this contribution, we analyze debond initiation and propagation in Representative Volume Elements (RVEs) of Uni-Directional (UD) composites and $[0^\circ_{m\cdot k\cdot 2L}, 90^\circ_{k\cdot 2L}, 0^\circ_{m\cdot k\cdot 2L}]$ laminates. Given a global reference frame with axis x, y and z, both types of composites are modeled as plates lying in the $x-y$ plane, with the through-the-thickness direction thus aligned with the z axis. The UD composite 0° direction is parallel to the y axis, while the cross-ply 0° direction is parallel to the x axis. Both composites are loaded in tension along the x axis, which thus corresponds to: transverse loading of the UD specimen; axial loading of the cross-ply specimen. In both composites, damage is present only in the form of fiber/matrix interface cracks, or debonds. In cross-plies, debonds are assumed to be present only in the central 90°. Given that: first, in the presence of a load in the x-direction, the y-strain due to Poisson's effect is very small; second, debond size is assumed to be considerably larger in the fiber than in the arc direction [1]; we can consider $2D$ models under plane strain conditions defined in the $x-z$

plane. UD composites and 90° plies are characterized by a regular microstructure following a square-packing configuration of fibers, built through the repetition of a one-fiber unit cell along the horizontal and the vertical direction. This unit cell is a square with the center occupied by one fiber of radius $R_f = 1\ \mu m$ and the rest of the element constituted by matrix. The size of the one-fiber unit cell is $2L \times 2L$, such that:

$$L = \frac{R_f}{2}\sqrt{\frac{\pi}{V_f}}, \tag{1}$$

where V_f is the fiber volume fraction, here assumed to be 60%. It is worth to specify at this point that the choice $R_f = 1\ \mu m$ is arbitrary and stems from the fact that the linear elastic solution, as the one considered in this article, is proportional to the geometrical dimensions of the model. Simplicity is thus the main reason for this choice. Also, V_f is always the same in the one-fiber unit cell and the entire RVE, i.e. no fiber clustering is analyzed in this work. In the case of cross-ply laminates, the 0° layer is homogenized with properties evaluated according to the Concentric Cylinders Assembly with Self-Consistent Shear (CCA-SCS) model [2, 3]. A glass fiber-epoxy system is considered for both UDs and cross-ply laminates. Material properties are reported in Table 1.

Table 1. Summary of mechanical properties of fiber, matrix and UD layer.

Material	$V_f\,[\%]$	$E_L\,[GPa]$	$E_T\,[GPa]$	$G_{LT}\,[GPa]$	$\nu_{LT}\,[-]$	$\nu_{TT}\,[-]$
Glass fiber	-	70.0	70.0	29.2	0.2	0.2
Epoxy	-	3.5	3.5	1.25	0.4	0.4
UD	60.0	43.442	13.714	4.315	0.273	0.465

The use of coupling conditions allows the study of a Repeating Unit Cells (RUC) of reduced size with respect to the corresponding RVE, which translates in a gain in terms of computational time and memory usage during the evaluation of Finite Element (FE) solution. The RVEs studied in this article are reported in Figure 1 with the corresponding RUC highlighted by dashed line (in blue in the online color version) and with symmetry and coupling conditions represented by rollers (). Details about the central one-fiber unit cell are shown in Figure 2. Notice that the analysis, in terms of stresses and Energy Release Rate (ERR), is conducted on this central one-fiber unit cell, both in the case of an undamaged and of a partially debonded fiber.
Nomenclature and main features of the RVEs studied are described in the following.

$\mathbf{n \times k - free}$, Figure 1(a): UD composite with thickness $t_{0^\circ} = k \cdot 2L$, where k is the number of fiber "rows" in the vertical (through-the-thickness) direction and $2L$ the side length of the one-fiber unit cell as defined in Equation 1. Debonds appear only in the central fiber "row" every $n-1$ fully bonded fibers on alternating sides of the partially debonded fiber, where n is the number of fiber present in the RUC along the horizontal direction.

$\mathbf{n \times k - coupling}$, Figure 1(b): UD composite with infinite thickness. Debonds appear every $k-1$ fully bonded fibers along the vertical direction in a fiber "column", fiber "columns" containing debonds appear every $n-1$ "columns" of fully bonded fibers. Debonds are placed on the same side of the partially debonded fiber inside the same fiber "column", while they appear on alternating sides between one fiber "column" with damage to the next. The RUC has thus n fibers in the horizontal and k fibers in the vertical direction. Conditions of coupling of the vertical displacement are applied on the top side.

$\mathbf{n \times k - asymm}$, Figure 1(c): UD composite with infinite thickness. Debonds appear every $k-1$ fully bonded fibers along the vertical direction in a fiber "column", fiber "columns" containing debonds appear every $n-1$ "columns" of fully bonded fibers. Debonds are placed on opposite sides of the partially debonded fiber inside the same fiber "column" and they appear on alternating sides between one fiber "column" with damage to the next. The RUC has thus n fibers in the horizontal and k fibers in the vertical direction. The following set of conditions is applied to the upper boundary:

$$\begin{aligned} u_z(x, kL) - u_z(0, kL) &= -\left(u_z(-x, kL) - u_z(0, kL)\right) \\ u_x(x, kL) &= -u_x(-x, kL) \end{aligned} \tag{2}$$

which represent conditions of anti-symmetric coupling [4].

$\mathbf{n \times k - m \times t_{90^\circ}}$, Figure 1(d): Cross-ply laminate with 90° layer thickness $t_{90^\circ} = k \cdot 2L$ and 0° layer thickness $t_{0^\circ} = m \cdot t_{90^\circ}$. k is the number of fiber "rows" in the vertical (through-the-thickness) direction of the 90° layer and $2L$ the side length of the one-fiber unit cell as defined in Equation 1. Debonds are present only in the central fiber "row" of the 90° layer every $n-1$ fully bonded fibers on alternating sides of the partially debonded fiber, where n is the number of fiber present in the RUC along the horizontal direction.

Every RUC is symmetric with respect to the horizontal (x) direction, thus only half of it is modeled in the FE solution through the use of symmetry boundary conditions on the bottom side. Conditions of coupling of the horizontal displacement are applied on the left and right side, to model the repetition of the RUC along the horizontal direction. A tensile load is applied on the right and left side in the form of displacement $\bar{u}_x = \bar{\varepsilon}_x nL$ with $\bar{\varepsilon}_x = 1\%$. The debond has a size of $2\Delta\theta$ (see Figure 2), with $\Delta\theta \geq 0$ ($\Delta\theta = 0$ is the case of no damage at all). For large debonds ($\Delta\theta \geq 60^\circ - 80^\circ$), a region called *contact zone*, of size $\Delta\Phi$ to be determined by the solution itself, appears at the crack tip. Correct resolution of this behavior requires the imposition of conditions of non-interpenetration of the crack faces. Crack faces contact is assumed to be frictionless.

The FE solution is evaluated using Abaqus [5] using second order, 2D, plane strain triangular (CPE6) and rectangular (CPE8) elements. To correctly resolve the singularity at the crack tip, a regular mesh of only rectangular elements is used with almost unitary aspect ratio and angular

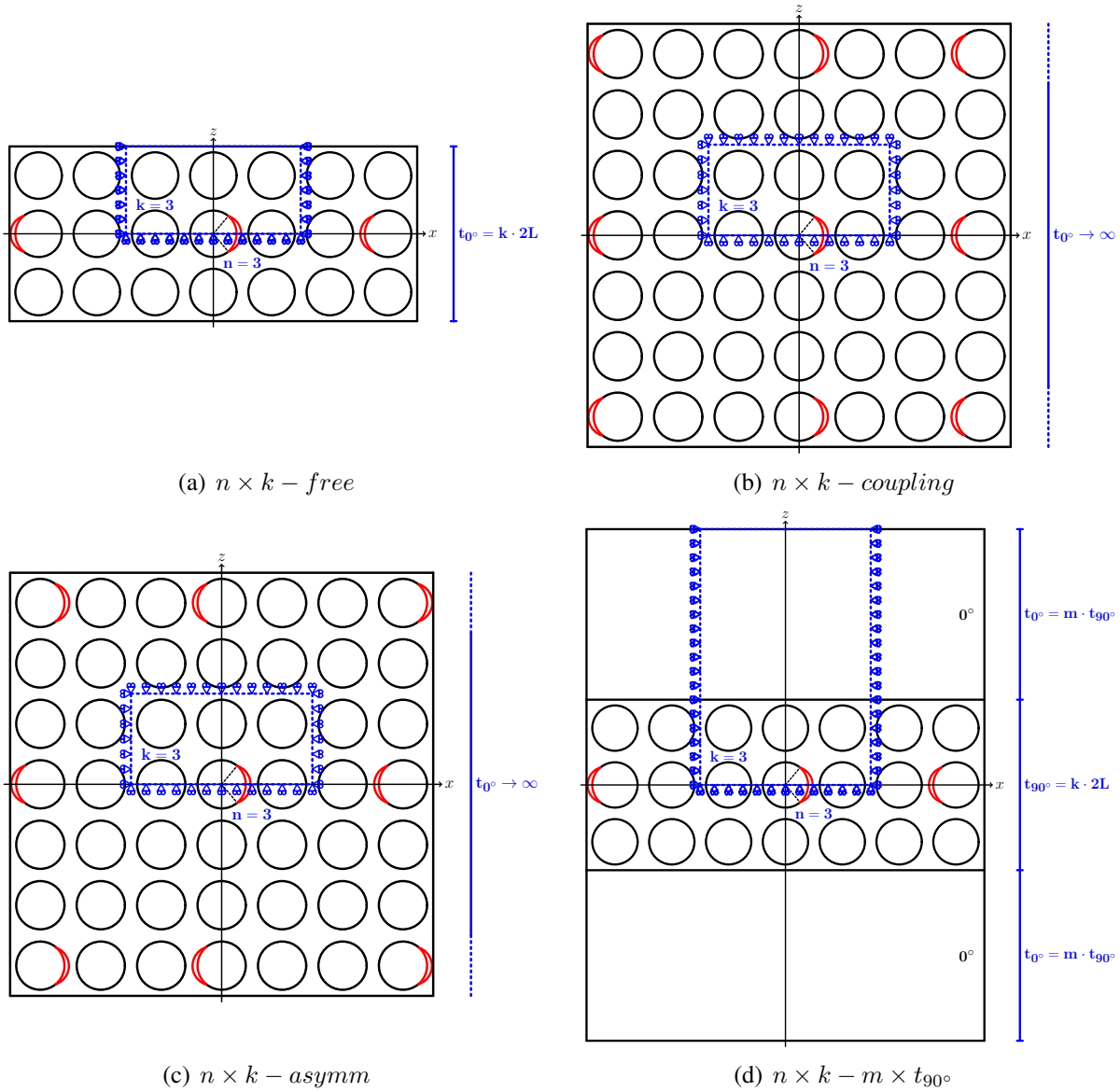

(a) $n \times k - free$

(b) $n \times k - coupling$

(c) $n \times k - asymm$

(d) $n \times k - m \times t_{90^\circ}$

Figure 1. Composite RVEs and corresponding RUCs analyzed.

size $\delta = 0.05^\circ$. The crack faces are represented as element-based surfaces with frictionless small-sliding contact pair interaction.

Mode I ERR is underestimated with the Virtual Crack Closure Technique (VCCT) [6] for very small debonds (see Figure 3), due to the high $\frac{\delta}{\Delta\theta}$ ratio. Thus, for $\Delta\theta < 10^\circ$, G_{TOT} is evaluated using the J-integral [7], G_{II} with the VCCT and G_I as $G_{TOT} = G_I + G_{II}$; for $\Delta\theta \geq 10^\circ$ only the VCCT is used. Validation of the model is performed with respect to BEM results of [8, 9]; the order of accuracy of the results (differences $\leq 5\%$ are not significant) is discussed in [10].

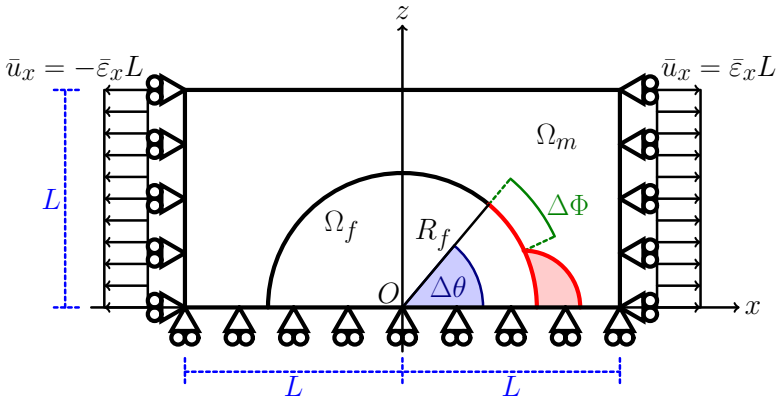

Figure 2. One-fiber unit cell and main parameters characterizing the debonding process.

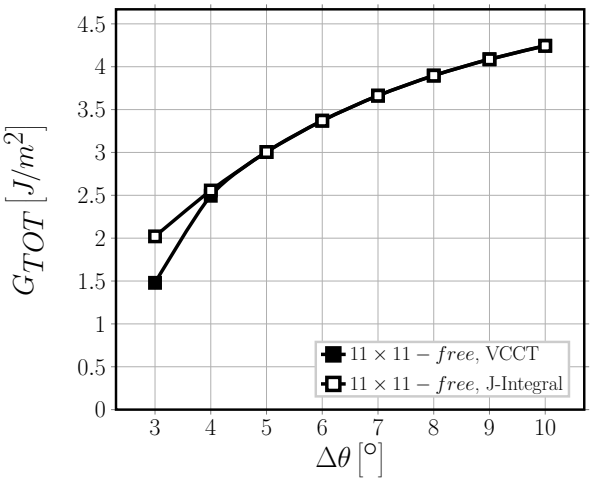

Figure 3. Comparison of total ERR of $11 \times 11 - free$ evaluated respectively with VCCT and J-integral.

3. STRESS-BASED ANALYSIS OF DEBOND INITIATION

The distribution of stresses at the fiber/matrix interface is analyzed in models $1 \times k - free$ and $1 \times k - 1 \cdot t_{90^\circ}$ with $k = 1, 3, 11, 201$ and $\Delta\theta = 0^\circ$, i.e. the undamaged case. Some selected stress components are analyzed, based on their relevance in previous studies on debond initiation and growth: the radial σ_{rr} and shear $\tau_{r\psi}$ stress [11] (Fig. 4(a) and Fig. 4(b)), the Local Hydrostatic Stress (LHS, following the notation of [12]) σ_{LHS} [13, 14] (Fig. 4(c) and Fig. 4(d)), the local von Mises stress σ_{vM} [15] (Fig. 4(e) and Fig. 4(f)), the Local Maximum Principal Stress (LMPS, following the notation of [12]) σ_{LMPS} [16] (Fig. 4(g) and Fig. 4(h)). In plane strain conditions there exists an out-of-plane axial component of the stress (σ_{yy} in our notation): in order to study the importance of this out-of-plane component (tri-axial stress state, see [17]), σ_{LHS}, σ_{vM} and σ_{LMPS} are evaluated both neglecting (index $2D$) and considering (index $3D$) σ_{yy}.

It is possible to observe that:

1. for all stress components, no significant difference is present between the different RUCs for $\psi \leq 10°$;
2. for all stress components, no difference can be observed by increasing k when $k \geq 3$;
3. for all stress components, no difference can be observed between $1 \times k - free$ and $1 \times k - 1 \cdot t_{90°}$ for $k \geq 3$;
4. at $\psi = 0°$ (i.e. the intersection between fiber/matrix interface and horizontal axis); the shear stress $\tau_{r\psi}$ (Fig. 4(b)) is 0 while the radial stress σ_{rr} (Fig. 4(a)) is at its maximum;
5. comparison of Fig. 4(c) with Fig. 4(d) shows that the out-of-plane stress σ_{yy} has only a marginal effect on the local hydrostatic stress σ_{LHS}: the distribution remains the same, while the peak value is reduced from $270\ [MPa]$ in Fig. 4(c) to $250\ [MPa]$ in Fig. 4(d) by considering σ_{yy};
6. comparison of Fig. 4(e) with Fig. 4(f) shows a remarkable effect of the out-of-plane stress σ_{yy} on the von Mises stress: if σ_{yy} is neglected, σ_{vM} presents a maximum of $287\ [MPa]$ at $\psi = 0°$, slightly higher than the value of σ_{LHS} (neglecting σ_{yy}) of $270\ [MPa]$ at $\psi = 0°$; if σ_{yy} is considered, the peak value of σ_{vM} is shifted to $\psi \sim 20°$ and reduced to $186\ [MPa]$ while at $\psi = 0°$ σ_{vM} is reduced to $\sim 110\ [MPa]$, significantly lower than $\sigma_{LHS} = 250\ [MPa]$ at $\psi = 0°$ (considering σ_{yy});
7. comparison of Fig. 4(g) with Fig. 4(g) shows that the Local Maximum Principal Stress is practically unaffected by the out-of-plane stress σ_{yy};
8. σ_{rr}, $\sigma_{LHS,2D}$, $\sigma_{LHS,3D}$, $\sigma_{vM,2D}$, $\sigma_{LMPS,2D}$ and $\sigma_{LMPS,3D}$ all reach their peak value at $0°$ and $180°$ and decrease to 99% the peak value between $2°$ and $8°$, to 95% the peak value between $6°$ and $12°$ and to 90% the peak value between $8°$ and $15°$.

Based on the previous considerations, it is reasonable to assume that a stress-based criterion would predict, irrespectively of the specific criterion chosen, the onset of an interface crack at $0°$ or $180°$ with an initial size at least comprised in the range $2° - 8°$ (1% margin) and likely in the range $6° - 12°$ (5% margin).

4. ENERGY-BASED ANALYSIS OF DEBOND PROPAGATION

We assume an expression for the critical Energy Release Rate G_c at the interface of the form [18, 11]:

$$G_c = G_{Ic}\left(1 + \tan^2\left(\left(1 - \lambda\right)\Psi_G\right)\right), \quad \Psi_G = tan^{-1}\left(\sqrt{\frac{G_{II}}{G_I}}\right), \tag{3}$$

where Ψ_G is the energy-based phase angle, G_{Ic} is the Mode I critical ERR (material property) and λ the mode mixity sensitivity parameter (material property, usually $0.2 \leq \lambda \leq 0.35$)[1]. By calculating Mode I, Mode II and total ERR and equating the expression of G_c in Eq. 3 to G_{TOT}, it is possible to estimate the value of G_{Ic} for different values of the assumed initial debond size $\Delta\theta_0$ and of the parameter λ (Figure 5). The estimation is performed using a restricted set of RUCs: $11 \times 1 - free$, $11 \times 11 - free$, $11 \times 1 - 1 \cdot t_{90^\circ}$ and $11 \times 11 - 1 \cdot t_{90^\circ}$.

Remarkably, neither RUC configuration nor λ affects G_{Ic} significantly for small initial flaw size ($\Delta\theta_0 < 10^\circ$). Based on the considerations of the previous section, we can expect the initial flaw to be in the range $2^\circ - 12^\circ$ ($1 - 5\%$ margin): comparing this with the results of Figure 5, we can assume G_{Ic} to be in the range $2 - 4.5 \left[\frac{J}{m^2}\right]$, while $0.2 \leq \lambda \leq 0.35$.

5. CONCLUSIONS

We are looking forward to receiving your contributions for this conference.

ACKNOWLEDGEMENTS

Luca Di Stasio gratefully acknowledges the support of the European School of Materials (EUSMAT) through the DocMASE Doctoral Programme and the European Commission through the Erasmus Mundus Programme.

References

[1] H. Zhang, M.L. Ericson, J. Varna, and L.A. Berglund. Transverse single-fibre test for interfacial debonding in composites: 1. experimental observations. *Composites Part A: Applied Science and Manufacturing*, 28(4):309–315, January 1997.

[2] Z. Hashin. Analysis of composite materials—a survey. *Journal of Applied Mechanics*, 50(3):481, 1983.

[3] R.M. Christensen and K.H. Lo. Solutions for effective shear properties in three phase sphere and cylinder models. *Journal of the Mechanics and Physics of Solids*, 27(4):315–330, August 1979.

[4] Luca Di Stasio, Janis Varna, and Zoubir Ayadi. Growth of interface cracks on consecutive fibers: on the same or on the opposite sides? *Materials Today: Proceedings*, In Press.

[5] Simulia, Providence, RI, USA. *ABAQUS/Standard User's Manual, Version 6.12*, 2012.

[6] Ronald Krueger. Virtual crack closure technique: History, approach, and applications. *Applied Mechanics Reviews*, 57(2):109, 2004.

[1] λ governs the influence of mode ratio $\frac{G_{II}}{G_I}$ on G_c such that: for $\lambda = 1$, $G_c = G_{Ic}$; for $\lambda = 0$, $G_c = G_{Ic}\left(1 + \frac{G_{II}}{G_I}\right)$.

[7] J. R. Rice. A path independent integral and the approximate analysis of strain concentration by notches and cracks. *Journal of Applied Mechanics*, 35(2):379, 1968.

[8] Federico París, Elena Correa, and Vladislav Mantič. Kinking of transversal interface cracks between fiber and matrix. *Journal of Applied Mechanics*, 74(4):703, 2007.

[9] C. Sandino, E. Correa, and F. París. Numerical analysis of the influence of a nearby fibre on the interface crack growth in composites under transverse tensile load. *Engineering Fracture Mechanics*, 168:58–75, December 2016.

[10] Luca Di Stasio, Janis Varna, and Zoubir Ayadi. Energy release rate of the fiber/matrix interface crack in UD composites under transverse loading: effect of the fiber volume fraction and of the distance to the free surface and to non-adjacent debonds. *Theoretical and Applied Fracture Mechanics*, 103, October 2019.

[11] V. Mantič. Interface crack onset at a circular cylindrical inclusion under a remote transverse tension. application of a coupled stress and energy criterion. *International Journal of Solids and Structures*, 46(6):1287–1304, March 2009.

[12] P.A. Carraro and M. Quaresimin. Modeling the crack initiation in unidirectional laminates under multiaxial fatigue loading1. In *Modeling Damage, Fatigue and Failure of Composite Materials*, pages 357–375. Elsevier, 2016.

[13] L.E. Asp, L.A. Berglund, and R. Talreja. A criterion for crack initiation in glassy polymers subjected to a composite-like stress state. *Composites Science and Technology*, 56(11):1291–1301, January 1996.

[14] L.E. Asp, L.A. Berglund, and R. Talreja. Prediction of matrix-initiated transverse failure in polymer composites. *Composites Science and Technology*, 56(9):1089–1097, January 1996.

[15] Luis Pablo Canal, Carlos González, Javier Segurado, and Javier LLorca. Intraply fracture of fiber-reinforced composites: Microscopic mechanisms and modeling. *Composites Science and Technology*, 72(11):1223–1232, June 2012.

[16] P.A. Carraro and M. Quaresimin. A damage based model for crack initiation in unidirectional composites under multiaxial cyclic loading. *Composites Science and Technology*, 99:154–163, July 2014.

[17] Leif E. Asp, Lars A. Berglund, and Peter Gudmundson. Effects of a composite-like stress state on the fracture of epoxies. *Composites Science and Technology*, 53(1):27–37, January 1995.

[18] J.W. Hutchinson and Z. Suo. Mixed mode cracking in layered materials. In *Advances in Applied Mechanics*, pages 63–191. Elsevier, 1991.

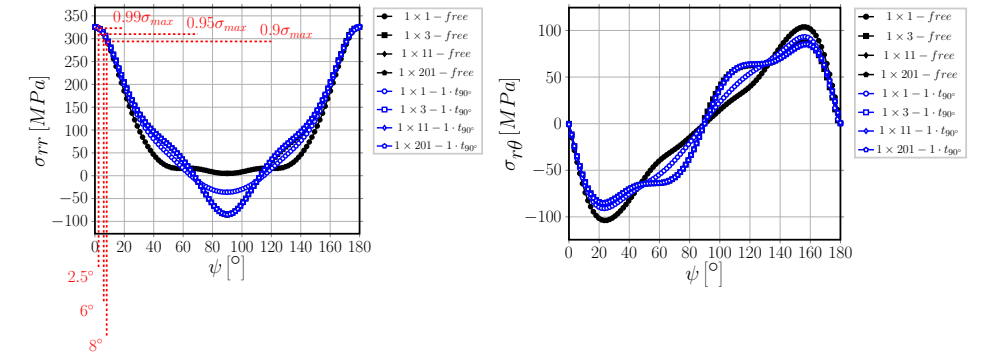

(a) σ_{rr}

(b) $\tau_{r\psi}$

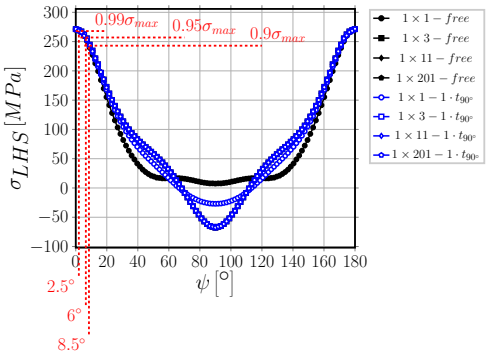

(c) $\sigma_{LHS,2D}$

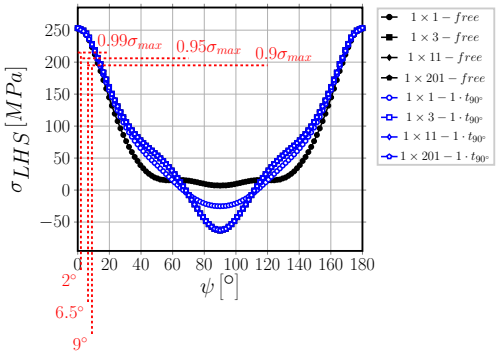

(d) $\sigma_{LHS,3D}$

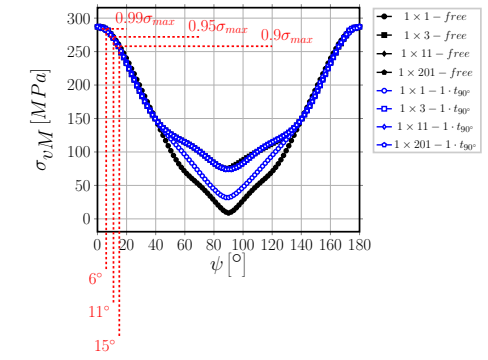

(e) $\sigma_{vM,2D}$

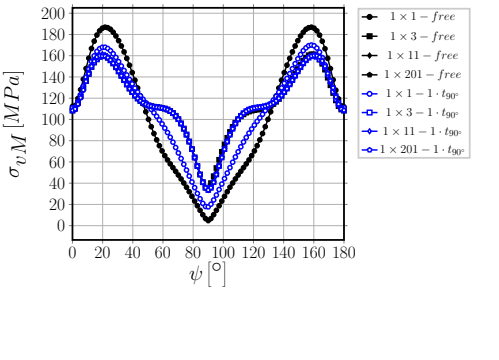

(f) $\sigma_{vM,3D}$

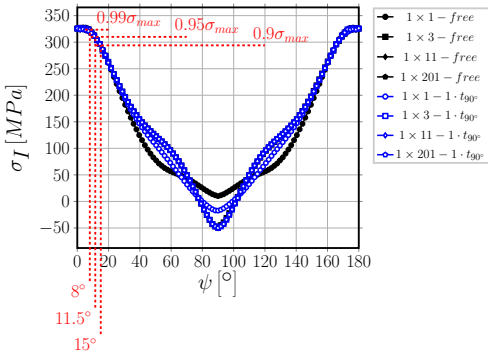

(g) $\sigma_{LMPS,2D}$

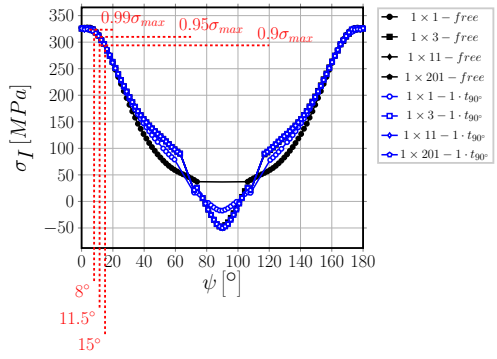

(h) $\sigma_{LMPS,3D}$

Figure 4. Stress distribution at the fiber/matrix interface in the absence of damage.

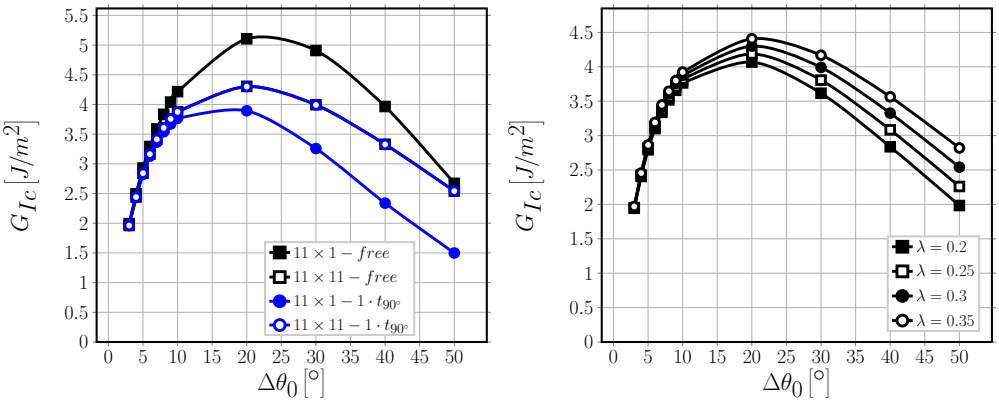

(a) $\lambda = 0.3$ (b) $11 \times 11 - 1 \cdot t_{90^\circ}$

Figure 5. Estimated values of G_{Ic} assuming different values of initial debond size, for different RUCs and varying λ.